Int J Fract (2019) 216:161–171
https://doi.org/10.1007/s10704-019-00350-4

ORIGINAL PAPER

A fracture model for exfoliation of thin silicon films

Martin Ward · Michael Cullinan

Received: 26 September 2018 / Accepted: 6 February 2019 / Published online: 14 February 2019
© Springer Nature B.V. 2019

Abstract The direct exfoliation of thin films from silicon wafers has the potential to significantly lower the cost of flexible electronics while leveraging the performance benefits and established infrastructure of traditional wafer-based fabrication processes. However, controlling the thickness and uniformity of exfoliated silicon thin films has proven difficult due to a lack of understanding and control over the exfoliation process. This paper presents a new silicon exfoliation process and model which enables accurate prediction of the thickness and quality of the exfoliated thin-film based on the exfoliation process parameters. This model uses a parametric, finite element, linear elastic fracture mechanics study with nonlinear loading to determine how each process parameter affects the crack propagation depth. A metamodel is then constructed from the results of numerous simulations to inform the design and operation of a novel exfoliation tool and predict thickness of produced films. In order to manufacture uniform, high-quality films, the tool creates a controlled peeling load that is able to propagate a crack through the silicon in a controlled manner. Finally, exfoliated silicon samples produced with the prototype tool are evaluated and compared to metamodel projections, confirming the ability of the tool to steer crack trajectory within ± 3 microns of the crack depth predictions.

M. Ward · M. Cullinan (✉)
Department of Mechanical Engineering, University of Texas at Austin, Austin, TX 78712, USA
e-mail: michael.cullinan@austin.utexas.edu

Keywords Exfoliation · Single crystal silicon · Finite element analysis · Spalling

1 Introduction

In recent years, flexible electronic devices have gained increased traction in the market and have become significantly more sophisticated (Pang et al. 2013). Notable areas of development include wearable electronics (Kim et al. 2014; Ying et al. 2012), and photovoltaics (Pudasaini et al. 2014; Ahn et al. 2017; Pagliaro et al. 2008). To achieve flexibility, these systems generally employ new materials and fabrication techniques that are inherently flexible, such as thin-film solar cells or organic or oxide-based (Fortunato et al. 2012) thin-film-transistors built on polymer substrates (Pagliaro et al. 2008). These solutions either result in lower performance or place the rigid traditional complementary metal–oxide–semiconductor (CMOS) fabricated integrated circuits on a separate rigid module or in a discretized array (Takei et al. 2010). The use of thin-film monocrystalline silicon (c-Si) could improve the performance of these flexible electronic devices by allowing high-quality CMOS devices to be fabricated directly on flexible substrates, thus creating opportunities for development of entirely new applications of flexible electronics.

Exfoliation is a promising method for creating cost-effective thin-film c-Si while leveraging existing CMOS infrastructure. This method of thin-film layer

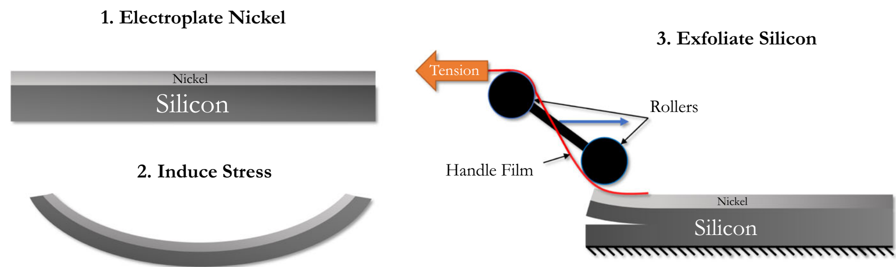

Fig. 1 Controlled peeling process diagram

transfer often referred to as "spalling", "large-area lift-off", and "kerfless wafering", all describing a process in which a stress field created by a tensile film deposited on top of a bulk substrate propagates a brittle fracture just beneath the surface of the substrate. This phenomenon often appears in other fields as a mode of failure. For example, the coating of dissimilar materials coupled with thermal- or deposition-related stresses can cause the structure to fracture and fail in many semiconductor manufacturing processes. The first mention of exfoliation as a method of manufacturing thin c-Si films was made in a patent by Tanielian et al. (1986), though results were never discussed in literature. The first demonstration of exfoliation of thin-film silicon in literature was performed by Dross et al. (2007) using printed metal pastes as the tensile layer which were then dried and annealed. Exfoliation occurred spontaneously due to an excess of stress created by the mismatch in coefficients of thermal expansion (CTE) as the assembly cooled from the annealing temperature. Other methods of exfoliation developed by R. Rao and L. Mathew from University of Texas at Austin (Rao et al. 2011; Mathew and Jawarani 2010; Zhai et al. 2012) and D. Shahjerdi and S. Bedell from IBM (Bedell et al. 2012, 2013a, b; Shahrjerdi and Bedell 2013; Shahrjerdi et al. 2012) provide more control over the stress in the tensile film, and therefore the resulting silicon film. Both methods deposit a layer of nickel on top of the silicon wafer with a residual stress that is just below what is required to spontaneously initiate a crack. Then, an additional load is applied to propagate the crack. Rao and Mathew used a wedge tool to apply load to the crack tip while Shahjerdi and Bedell used adhesive tape as a peeling handle. The method of exfoliation presented here combines features from those described above but adds a critical element of control to the external applied loading.

The work presented in this paper is a model formulation to better understand the exfoliation process and accurately control the parameters that affect the thickness and quality of the resulting films. The exfoliation phenomenon in silicon is an example of brittle fracture. Due to the silicon wafer's single crystal structure and very brittle nature, it can be modeled using linear elastic fracture mechanics. The goal of the model is to be able to predict the crack propagation depth for a given loading. To do this, we focus on the Mode I (K_I) and Mode II (K_{II}) stress intensity factors (SIFs). The SIFs are a means of estimating the stress fields at the crack tip where K_I describes an opening mode of the crack and K_{II} describes a shearing mode. Previous work by Thouless et al. (1987) in studying interfacial fracture phenomenon indicates that, for a given elastic system, a crack has a stable propagation depth that is controlled by a tendency of K_{II} towards zero. The model presented here provides insight as to how a tool could be designed to use this phenomenon to steer the crack to a desired depth and, thereby, create silicon films of a desired thickness. A diagram of the proposed mechanism is shown in Fig. 1, where control of handle tension and roller height can be used to modulate the stress fields around the crack tip.

A layer of nickel is electrodeposited on a c-Si wafer and a tensile stress designed to be just below the threshold for spontaneously initiating a crack is induced thermally. The wafer is then fixed to a rigid substrate and the film is exfoliated. The controlled peeling concept uses two idler rollers to control the angle and tension in the handle film, which is fixed to ground at one end and to the nickel tensile layer at the other. The rollers are then moved across the wafer by a linear actuator. This provides control of the rate at which energy is added to the crack. The tension in the film and the height and orientation of the rollers can be adjusted to alter the loads applied to the tensile layer and then to the crack tip. This load is used to steer the crack. A series of experiments were performed to test the capabilities of the tool and performance of the model.

In this paper, we first review the analytical background of the thin-film fracture problem in Sect. 2. We will then define and construct a parametric FEA model of the exfoliation process in Sect. 3. The results of the FEA model and their integration into a metamodel will then be presented in Sect. 4. Finally, experimental results from the new exfoliation tool will be presented in Sect. 5 and compared to the metamodel predictions.

2 Fracture system and analytical background

Efforts to understand the exfoliation phenomenon began mainly as a means of avoiding the failure of coated films in a variety of applications including electronic device manufacturing (Cannon et al. 1985; Suo and Hutchinson 1989; Xu et al. 1993). It was observed in literature that under certain conditions, interfacial fractures follow a trajectory down into the substrate and then level out at a depth characteristic of the system and the loading conditions. An analytical approach to calculating the characteristic propagation depth was developed by Drory et al. (1988) and Suo and Hutchinson (1989). Their method resolves a residual stress in a film as an edge load and moment. The stress fields corresponding to this loading condition were found by relating the stresses in the beam far from the crack tip to the strain energy release rate. The SIFs can then be calculated, resulting in the following relations for a given elastic system (Suo and Hutchinson 1989):

$$K_I = \frac{P}{\sqrt{2Uh}}\cos(\omega) + \frac{M}{\sqrt{2Vh^3}}\sin(\omega+\gamma) \tag{1}$$

and

$$K_{II} = \frac{P}{\sqrt{2UH}}\sin(\omega) - \frac{M}{\sqrt{2Vh^3}}\cos(\omega+\gamma), \tag{2}$$

where P is the resolved edge force, M is the resolved edge moment, and h is the film thickness. Constants U, V, and γ are dimensionless quantities describing the elastic energy in the system, and ω is a dimensionless function of the elastic dissimilarity of the materials and the crack depth. A derivation of these equations is given in the appendix of Suo and Hutchinson (1989). The numerical solution to Eqs. (1) and (2) provides a map of the SIFs with respect to crack depth. This solution can be combined with the criterion that stable crack propagation occurs when $K_{II} = 0$ and $K_I = K_{Ic}$ to provide the characteristic crack depth for exfoliation, as used by Bedell et al. (2013a).

With this model, exfoliation film thicknesses can be predicted and, to some extent, controlled by varying the thickness and stress of the tensile layer. However, this solution is only valid for the given loading condition defined only by a residual stress in the film. Both examples of exfoliation methods from Bedell and Shahrjerdi and Mathew and Rao apply an additional load beyond the film stress to propagate the crack. Bedell and Shahrjerdi suggested this load to be negligible but did not quantify its effect. The modeling work presented here attempts to describe the effect of this extra load and show that it is non-trivial. The paper will also demonstrate that this effect can be used to add another method of controlling the exfoliation crack depth to the exfoliation process.

3 Parametric FEA model

The model presented in this paper is based on the analytical model described above where the criteria, $K_{II} = 0$ and $K_I = K_{Ic(100)}$, are used to describe stable propagation of the crack front, but adds an additional tension load and displacement condition that simulate the handle layer of the new controlled peeling tool that is described in Sect. 5.

3.1 Geometry and loading

The geometry for this analysis represents a 2D slice of a (100) silicon wafer with a film of nickel on top and a crack in the silicon that has reached steady-state. The nickel film has a thickness, t_f, and the crack has a length, a, and is at a depth, d, below the surface of the silicon. The crack is propagating in the $\langle 100\rangle$ direction and the slice is taken perpendicular to that so that it represents a $\{100\}$ plane. A plane strain condition is assumed due to the large out-of-plane thickness and constant out-of-plane loading (Fig. 2).

A symmetry condition is assumed far ahead of the crack, beyond where the stresses have reached equilibrium. During testing, the wafer was fixed by adhering it to a rigid glass slide with double-sided polyimide tape. The base of the wafer was correspondingly fixed in the simulation, removing the contributions of sub-

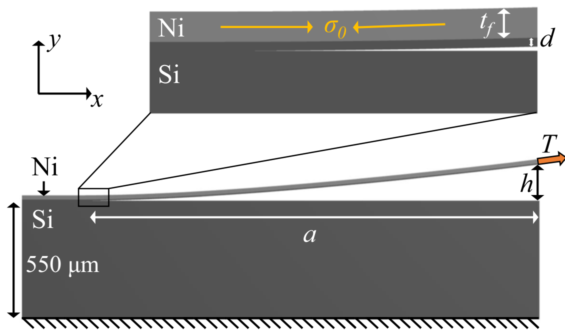

Fig. 2 Geometry and loading setup for FEA analysis

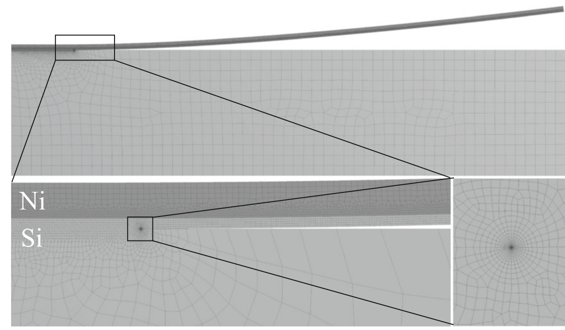

Fig. 3 Overview of sample meshing and detail of crack tip area

strate bending to the final stress state that are described in the analytical work of Drory et al. (1988) and Suo and Hutchinson (1989). The height of the silicon body is 550 µm, a representative thickness for the tested 100 mm diameter wafers. Due to the fixed constraint, the substrate thickness is not a significant factor in the results.

The residual stress in the nickel layer is introduced as a uniform uniaxial initial stress state, σ_0, in the x-direction, which is then allowed to relax for one load step. The actual stress induced in the electroplated film is biaxial and can vary throughout the film thickness. However, the out-of-plane stress caused by the film is effectively constant throughout the bulk of the wafer and, therefore, does not invalidate the plane-strain assumption.

A tension load, T, is applied to the end of the exfoliated film where the handle layer is attached. Due to the resulting effective infinite thickness in the z-direction in the model, the tension load was applied as an intensive pressure, but is later described as its resolved force at the middle cross-section of the wafer. A vertical displacement, h, is also applied to the end of the exfoliated film to simulate contact with the tool roller.

A 2-dimensional finite element model was created using ANSYS Design Modeler with special attention paid to the bodies that control the mesh around the crack tip and to the scale of the smallest features in the model. The geometry was imported into ANSYS Mechanical 18.1 and the region around the crack tip was carefully meshed as a series of radially divided concentric circles to conform to ANSYS requirements for their fracture mechanics tools. A mesh convergence study was performed to confirm the meshing around the crack tip was sufficient. Figure 3 shows the concentric mesh features that define the crack tip area.

The number of elements spanning the thin beams of nickel and silicon were defined explicitly and included in the convergence study. The mesh geometry and connections are manually defined at the crack tip to ensure reliable integration of the stress state around the tip. The mesh was set up so that the crack depth and nickel thickness could be varied parametrically and the mesh would be dynamically updated. All elements are ANSYS PLANE183 elements, and nonlinear effects and large deflections were enabled to accurately capture the deflection of the long beam behind the crack.

3.2 Materials

The simulation consists of two materials, single-crystal silicon and nickel electroplated from a sulfamate bath. The wafers used for the exfoliation tests are (100) orientation and are exfoliated in a ⟨100⟩ direction, meaning that the plane of the model also represents a {100} plane with the x and y axes also in the ⟨100⟩ directions. Therefore, a ⟨100⟩ isotropic assumption was made for this model. This assumption allows the correct material properties to be aligned along the x and y axes and the primary loading directions. In order to test the validly of this assumption, a series of simulations were performed while varying the isotropic elastic properties between those for the ⟨110⟩ and ⟨100⟩ directions to probe the effects on the crack trends. Comparisons were also made between anisotropic and isotropic simulations using the J-integral criterion (which ANSYS supports for anisotropic materials). The effect of this assumption appears to be minimal with respect to crack depth, a conclusion reached by other researchers as well (Calvez et al. 2014; Bouchard et al. 2013). However, a complete anisotropic analysis is planned in future work.

Table 1 Simulation material properties

	E (GPa)	ν	$K_{Ic(100)}$ (MPa $m^{1/2}$)
Silicon	169	.064	.75
Nickel	180	.31	

Silicon also exhibits anisotropy in its fracture toughness, which has been measured and calculated by several groups. The value of K_{Ic} varies greatly depending on the cleavage plane and the measurement type. Masolin et al. (2013) provides a review of these results with attention to their application to the exfoliation problem and gives a recommendation for the value of $K_{Ic(100)} = 0.75$ MPa $m^{1/2}$. Therefore, this value was used for $K_{Ic(100)}$ in the model presented in this paper.

The nickel tensile layer was deposited by a sulfamate electroplating process and the density as well as microstructural and elastic properties of the resulting material can vary depending on the plating conditions (Weil 1970). These conditions can also introduce anisotropy through columnar type structures (Weil 1970; Luo 2004). The nickel material properties used in these experiments were estimated using a key factor, current density, and data obtained by Luo (2004). The current density used was approximately 18 mA/cm^2 and the estimated Young's modulus is shown in Table 1. Poisson's ratio was assumed as bulk. However, a more complete characterization of the nickel material's properties is planned for future work.

3.3 Parametric strategy

A parametric study was performed to find the combination of parameters that result in a stable crack growth. The range of inputs were chosen to reflect those available during the experimentation process and to cover the range of desirable c-Si film thicknesses. The parameters were nondimensionalized with respect to the roller height, h, as it was kept constant throughout the modeling and experiments and they are listed in Table 2.

The concept underlying the parametric analysis is that for some combination of inputs (h, T, σ_0, t_f, a), there exisits a crack depth, d, that satisfies the $K_{II} = 0$ and $K_I = K_{Ic(100)}$ criterion. The model cannot be directly solved for this criterion, so it is explored iteratively while parametrically varying all the inputs. Varying the inputs was done with an optimal space-filling Latin Hypercube (LH) design of experiment (DOE) combined with an adaptive sampling method to create a refined response surface. In this method, the results of the LH design were used to create a Kriging response surface, which was then input into a multi-objective genetic algorithm configured to generate diverse and space-filling results around the objective criterion. These points were then input back into the FEA model and the solutions were added to the results of the LH DOE to create a more accurate response surface near the $K_{II} = 0$ and $K_I = K_{Ic(100)}$ criterion. This process was repeated until the response surface stabilized. The final response surface is a metamodel that can be solved to predict the crack depth for any valid combination of inputs.

4 Model results and metamodel

An example solution of the stress distributions of the system after the stress in the nickel has relaxed and the tension load and displacement condition have been applied is shown in Fig. 4. The distributions shown are for a median configuration of inputs where $h = 150$ (µm), $T/(h^2 E_{Ni}) \times 10^4 = 70$, $\sigma_0/E_{Ni} = 11.6$, $t_f/h = 0.115$, $a/h = 13.3$, $d/h = 0.033$. The color scales have been set to best display the stress fields near the crack tip. However, the maximum stress values shown in the legend are unreliable due to the singularity at the crack tip.

Figure 4a shows the von Mises stress state where one can see the general distribution of the stress and how the tensile stress in the nickel film relaxes to create a sharp concentration around the crack tip. Figure 4b shows the normal stress in the x-direction, where the stable uniaxial stress in the nickel after relaxation can be seen in the top-left corner. Interestingly, neutral axes are visible in both the silicon and nickel portions of the bilayer beam. Figure 4c shows the normal stress in the y-direction whose stress values that are much higher than the x-direction, as expected since this is the primary mode of fracture. It also displays typical single edge notched tension crack specimen stress fields for a plane strain assumption, which suggest that the crack will continue to propagate straight ahead. The SIFs are calculated using the stress fields around the crack tip. The FEA model was solved several thousand more times for the ranges of inputs shown in Table 2 and all the computed

Table 2 Simulation parameters

Inputs	Roller Height (µm) h	Handle Tension $T/(h^2 E_{Ni}) \times 10^4$	Nickel Stress $\sigma_0/E_{Ni} \times 10^4$	Nickel Thickness t_f/h	Crack Length a/h	Crack Depth d/h
Ranges	150	5-240	9-19	0.05-0.17	10-20	0-0.12
Outputs	K_I (MPa·m$^{1/2}$)			K_{II} (MPa·m$^{1/2}$)		
Targets	.75			0		

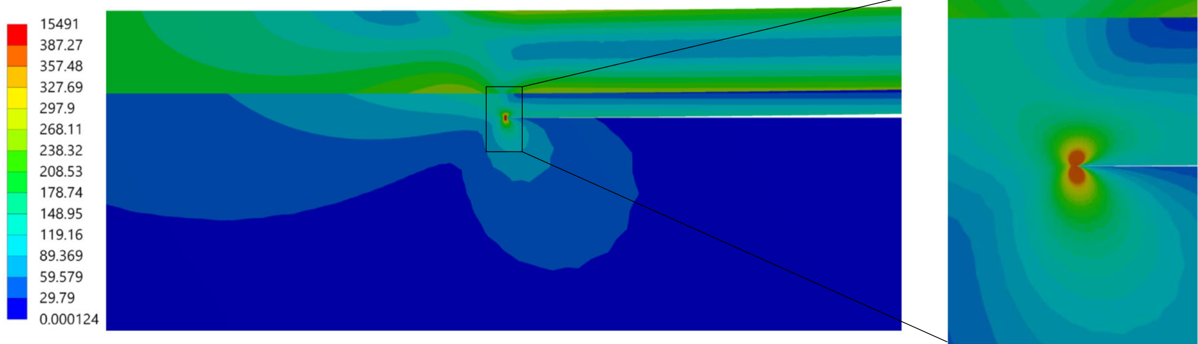

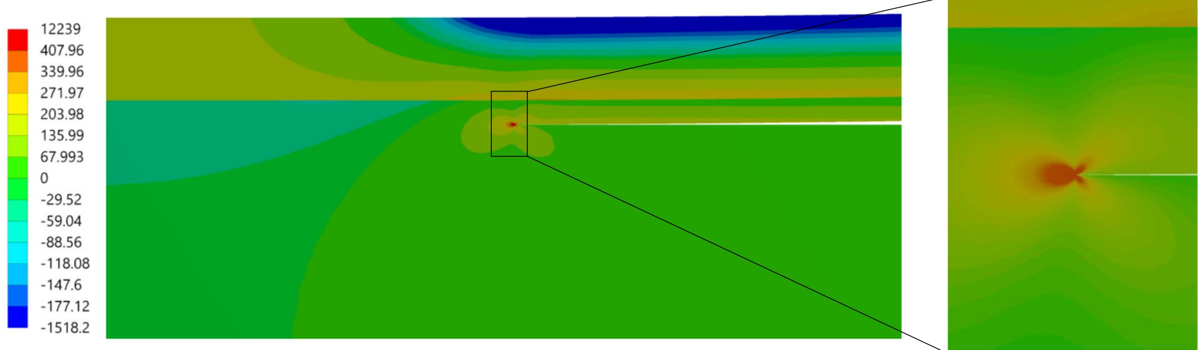

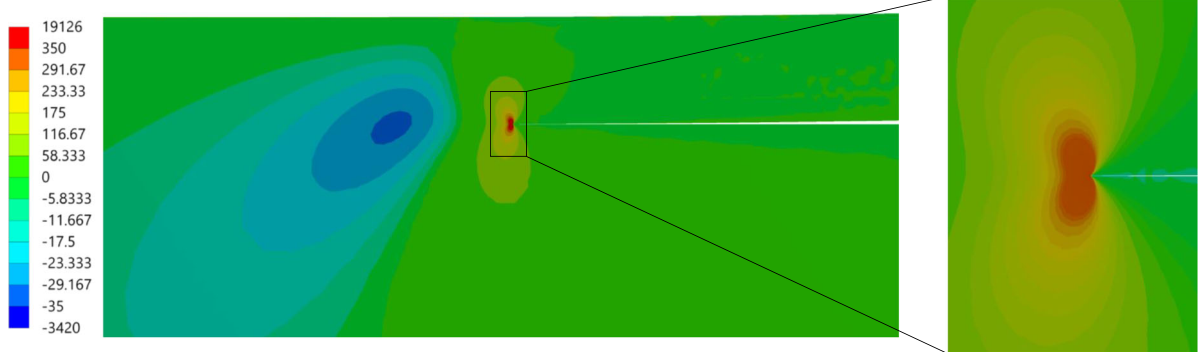

Fig. 4 Sample solution stress states

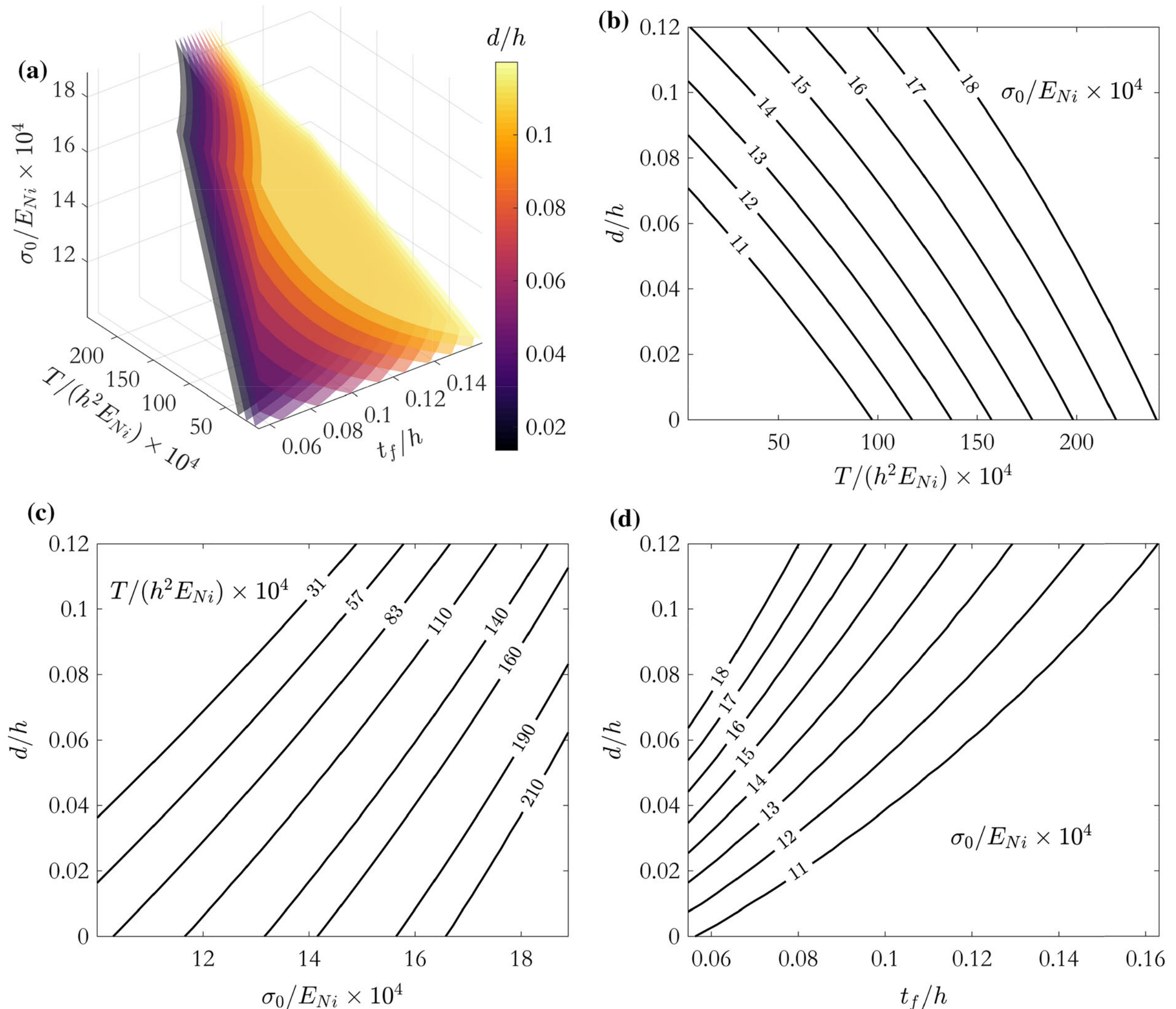

Fig. 5 Metamodel solutions for crack propagation space for $h = 150\,\mu\text{m}$ and $a/h = 13.3$. **a** Overview of the solution space. **b** Handle load versus crack depth for various film stresses. **c** Film stress versus crack depth for various handle loads. **d** Film thickness versus crack depth for various film stresses

SIFs are used to create the metamodel whose solution is shown in Fig. 5. The roller height and crack length were fixed to typical values of $150\,\mu\text{m}$ and $a/h = 13.3$ in order to create these visualizations, though the actual model is 6-dimensional.

The surfaces shown in Fig. 5a represent combinations of handle tension, nickel thickness, and nickel stress that satisfy the criteria stable crack depth, $K_{II} = 0$ and $K_I = K_{Ic(100)}$. These continuous solutions allow the metamodel to be used to predict the crack depth for a given set of system parameters. Figure 5b–d highlight different sections of the solution space. These plots reveal trends in the effect of each input. For example, increasing the tension tends to decrease the crack depth, which can be logically correlated with increasing tension essentially reducing the edge load created by the nickel. Increasing nickel thickness and nickel stress both drive the crack downward and increase the crack depth. The solution also shows that the handle tension is a more effective control input when nickel thickness and stress are low. This can be visualized by finding regions where the crack depth surfaces are most

Table 3 Comparison of experimentally measured crack depth with predicted crack depth

Sample	Nickel film thickness (μm)	Tension (N)	Nickel stress (MPa)	Measured crack depth (μm)	Predicted crack depth (μm)	Average error (μm)
1	14 ± 2.2	13 ± 1.2	260 ± 38	16 ± 3.3	14 ± 4.9	1.7
2	13 ± 1.9	21 ± 1.7	280 ± 43	10 ± 2.0	13 ± 4.4	2.9
3	18 ± 3.6	14 ± 2.4	240 ± 72	18 ± 6.2	22 ± 6.9	4.6
4	22 ± 3.1	15 ± 0.93	170 ± 27	12 ± 2.9	12 ± 3.5	2.7
5	11 ± 2.3	13 ± 3.9	290 ± 33	7.7 ± 2.2	10 ± 3.6	2.3
6	14 ± 3.0	8.8 ± 0.4	220 ± 24	5.2 ± 3.6	6.9 ± 3.5	1.8
7	22 ± 3.3	20 ± 0.25	150 ± 22	6.0 ± 1.0	7.3 ± 1.9	1.3
8	17 ± 1.5	50 ± 0.88	200 ± 22	7.7 ± 1.4	6.6 ± 2.2	1.2
9	16 ± 3.2	24 ± 7.1	220 ± 31	8.2 ± 3.7	12 ± 3.9	3.7
10	16 ± 3.2	17 ± 13	220 ± 29	13 ± 1.5	12 ± 4.6	3.3
11	13 ± 2.0	6.5 ± 0.55	250 ± 39	8.2 ± 4.2	12 ± 5.1	4.0
12	13 ± 2.3	2.9 ± 0.32	270 ± 28	12 ± 2.3	14 ± 4.7	2.3
13	17 ± 1.9	28 ± 0.8	210 ± 40	7.2 ± 3.1	12 ± 3.6	4.4
14	13 ± 1.6	57 ± 0.59	250 ± 37	4.2 ± 1.7	5.0 ± 2.6	1.1
15	18 ± 2.8	19 ± 1.8	210 ± 34	9.0 ± 2.8	12 ± 3.9	3.2
16	18 ± 3.3	8.0 ± 0.41	200 ± 31	9.7 ± 2.2	12 ± 3.6	2.7

Uncertainty shown is one standard deviation

perpendicular to the handle tension axis in Fig. 5a. If the stress is too low, however, deeper cracks are not possible, so the ideal region for control may be around medium stress levels and low nickel thickness to maximize the available control of the handle tension while still achieving a full range of crack depths.

5 Experimental results and comparison

Silicon wafers in (100) orientation and 100 mm diameter are prepared for exfoliation by vapor depositing titanium adhesion and nickel seed layers and then electroplating a nickel tensile layer in a sulfamate bath. The assembly is then heat-treated at a 200–250 °C for 30 min, after which the nickel layer shrinks and produces a residual tensile stress in the wafer. The wafer is then attached to a rigid glass slide using double-sided polyimide tape, which is then fixed in the exfoliation tool with a vacuum chuck. The handle layer is attached to the edge of the wafer and the tension is set and monitored with a load cell. The rollers are then moved over the wafer at a speed of approximately 8 mm/min to exfoliate the film. The wafers are measured before nickel plating, after nickel plating, and after exfoliation using a combination of dual KEYENCE LK-H207K differential laser displacement sensors for point measurements and LEXT OLS4100 confocal microscope for profile scans to build a full map of the wafer surface. The tensile stress is calculated using the profile scans and a modified Stoney's equation for silicon wafers (Janssen et al. 2009), which calculates the tensile stress in the nickel as a function of the film thickness, wafer thickness, and wafer curvature after annealing. The crack length, which is the distance to the crack tip to the point of contact with the roller, was estimated by creating a landmark in the exfoliated surface by varying the handle tension during exfoliation. The position of this mark was then combined with the position of the roller relative to the edge of the wafer, measured by a linear encoder on the tool, to calculate the crack length which was approximately 2 mm. Table 3 shows a distributed set of experiments that were performed at a constant roller height of 150 μm.

The values in the table represent the average of a profile scan across the wafer in the exfoliation direction. The metamodel predicts the crack depth with an average error of 2.7 μm, which is well within the average calculated uncertainty of 3.9 μm. The uncertainty in the predicted depth includes the uncertainties in the measurements of the nickel thickness and stress prop-

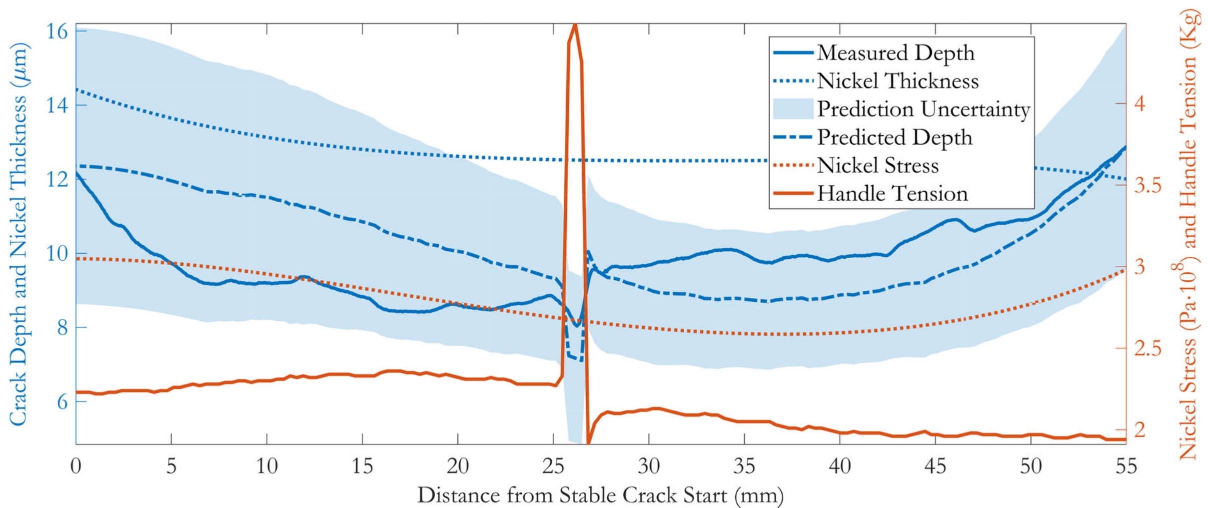

Fig. 6 Example profile of predicted depth versus measured depth across one wafer

agated through the metamodel combined with the variation recorded from multiple measurements across the wafer. Reducing the uncertainty in the measurements of nickel thickness and nickel stress would improve the value of the metamodel and could be achieved with advanced specialized metrology equipment. Additional understanding of how the processing conditions affect the crack depth predictions can be obtained by looking at the full profiles of each parameter as they vary across the wafer.

Figure 6 shows an example wafer profile comparing the predicted crack depth with the measured depth and provides the loading in the form of nickel film thickness and stress and handle tension as context. Once the the crack tip is sufficiently far from the wafer edges, the crack depth is independent of the crack tip's position relative to the wafer and variation in the depth is assumed to be caused by changes in the loading parameters. The peak in the center of the profile was a landmark created by varying the handle tension to help measure the crack length. This peak also highlights the system's sensitivity to handle tension and its potential for control. The prediction uncertainty is based on an analysis of the uncertainty in the measurements of the variables input into the metamodel and how those uncertainties propagate through the metamodel to the final crack depth prediction. The prediction appears to slightly overestimate the effect of the handle tension, but the predicted depth appears to follow the measured depth across the nickel thickness and stress trends well.

To demonstrate the control capabilities of the handle film tension, a similar test was performed but with a larger step change in tension. The profile for this test is shown in Fig. 7. Again, the metamodel appears to slightly overpredict the effect of the handle tension while accurately following the trends in the profile. In this case, the load change step was approximately 70 N which was predicted to induce a 6 μm change in crack depth. The actual change in depth was 4.3 μm. The discrepancy could be caused by a bias in the tension measurement system created by unaccounted for friction in the roller mechanism that is magnified by high tension loads. Both plots show non-uniformity in the measured crack depth profile that is unexplained by the nickel thickness, stress, and handle tension measurements. Therefore, this variation is also not demonstrated in the metamodel prediction. This may be caused by errors in the measurements or imperfections in the exfoliation tool's motion due to errors in the constraints and motion of the linear actuator and roller runout.

These results show that while the handle tension can be used to effectively influence the crack depth, other factors like the nickel thickness and stress also have a strong influence on the resulting crack depth and can produce nonuniformities in the final product. Increasing the uniformity of the nickel will improve results, but this is difficult to achieve with electroplating. Since electroplating is inexpensive, accurately measured nonuniformities could be countered by active control of the handle tension to produce cost-effective

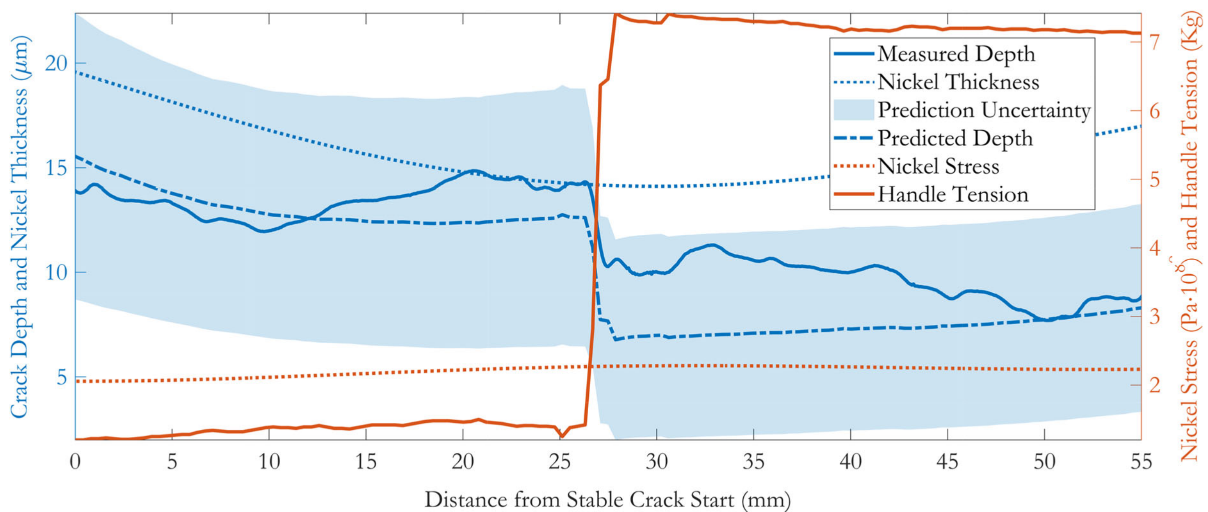

Fig. 7 Example wafer profile demonstrating crack depth control with step change

uniform films. Active handle tension control could also be used to create silicon films as thin as possible more easily. Without tension control, the nickel thickness and stress inputs would have to be targeted very near the point of interface failure. Tension control allows the inputs to be targeted at a thicker film, which is then brought to the minimum thickness by increasing the tension. The handle tension is much easier to adjust and control than the electroplating process and could produce thinner films and reduce the requirement for precise stress layer deposition. The design and construction of a high-precision, low-vibration version of the tool with active tension control that will minimize motion and tension measurement errors is underway. This tool will be used to test the limits of the exfoliated film thickness and improve uniformity and repeatability.

6 Conclusion

This paper presented a model and process for the exfoliation of c-Si thin-films with an electroplated nickel tensile layer. The FEA model was then used to create a metamodel to predict crack depth for a given system, and the new tool exploits the handle tension to control the crack depth. Together, the tool and exfoliation model provide the basis for cost-effective and scalable large-area monocrystalline thin-film photovoltaics and flexible devices.

Acknowledgements The authors acknowledge and thank Miaomiao Yang for her experience, effort, insight, and support in accomplishing this work. The authors thank Kirsten Cole Christopherson for her effort in completing these experiments. The authors would also like to thank Liam Conolly, Dipankar Behera, and Cheng Zhao for the informative discussions and technical expertise. This work is based upon work supported primarily by the National Science Foundation under Cooperative Agreement No. EEC-1160494. Any opinions, findings and conclusions or recommendations expressed in this material are those of the author(s) and do not necessarily reflect the views of the National Science Foundation.

References

Ahn J, Chou H, Banerjee SK (2017) Graphene-Al_2O_3-silicon heterojunction solar cells on flexible silicon substrates. J Appl Phys 121(16):163105. https://doi.org/10.1063/1.4981880

Bedell SW, Shahrjerdi D, Hekmatshoar B, Fogel K, Lauro PA, Ott JA, Sosa N, Sadana D (2012) Kerf–Less removal of Si, Ge, and III–V layers by controlled spalling to enable low-cost PV technologies. IEEE J Photovolt 2(2):141–147. https://doi.org/10.1109/JPHOTOV.2012.2184267

Bedell SW, Fogel K, Lauro P, Shahrjerdi D, Ott JA, Sadana D (2013a) Layer transfer by controlled spalling. J Phys D Appl Phys 46(15):152002. https://doi.org/10.1088/0022-3727/46/15/152002

Bedell SW, Shahrjerdi D, Fogel K, Lauro P, Hekmatshoar B, Li N, Ott J, Sadana DK (2013b) (Invited) cost-effective layer transfer by controlled spalling technology. ECS Trans 50(7):315–323. https://doi.org/10.1149/05007.0315ecst

Bouchard PO, Bernacki M, Parks D (2013) Analysis of stress intensity factors and T-stress to control crack propagation for kerf-less spalling of single crystal silicon foils.

Comput Mater Sci 69:243–250. https://doi.org/10.1016/j.commatsci.2012.10.033

Calvez D, Roqueta F, Jacques S, Bechou L, Ousten Y, Ducret S (2014) Crack propagation modeling in silicon: a comprehensive thermomechanical finite-element model approach for power devices. IEEE Trans Compon Packag Manuf Technol 4(2):360–366. https://doi.org/10.1109/TCPMT.2013.2293094

Cannon RM, Fisher RM, Evans AG (1985) Decohesion of thin films from ceramic substrates. In: MRS proceedings, vol 54. https://doi.org/10.1557/PROC-54-799

Drory MD, Thouless MD, Evans AG (1988) On the decohesion of residually stressed thin films. Acta Metall 36(8):2019–2028

Dross F, Robbelein J, Vandevelde B, Van Kerschaver E, Gordon I, Beaucarne G, Poortmans J (2007) Stress-induced large-area lift-off of crystalline Si films. Appl Phys A 89(1):149–152. https://doi.org/10.1007/s00339-007-4195-2

Fortunato E, Barquinha P, Martins R (2012) Oxide semiconductor thin-film transistors: a review of recent advances. Adv Mater 24(22):2945–2986. https://doi.org/10.1002/adma.201103228

Janssen G, Abdalla M, van Keulen F, Pujada B, van Venrooy B (2009) Celebrating the 100th anniversary of the Stoney equation for film stress: developments from polycrystalline steel strips to single crystal silicon wafers. Thin Solid Films 517(6):1858–1867. https://doi.org/10.1016/j.tsf.2008.07.014

Kim J, Lee M, Shim HJ, Ghaffari R, Cho HR, Son D, Jung YH, Soh M, Choi C, Jung S, Chu K, Jeon D, Lee ST, Kim JH, Choi SH, Hyeon T, Kim DH (2014) Stretchable silicon nanoribbon electronics for skin prosthesis. Nat Commun 5:5747. https://doi.org/10.1038/ncomms6747

Luo J (2004) Young's modulus of electroplated Ni thin film for MEMS applications. Mater Lett 58(17–18):2306–2309. https://doi.org/10.1016/j.matlet.2004.02.044

Masolin A, Bouchard PO, Martini R, Bernacki M (2013) Thermo-mechanical and fracture properties in single-crystal silicon. J Mater Sci 48(3):979–988. https://doi.org/10.1007/s10853-012-6713-7

Mathew L, Jawarani D (2010) Method of forming an electronic device using a separation-enhancing species. US patent US7749884B2. https://patents.google.com/patent/US7749884/en

Pagliaro M, Ciriminna R, Palmisano G (2008) Flexible solar cells. ChemSusChem 1(11):880–891. https://doi.org/10.1002/cssc.200800127

Pang C, Lee C, Suh KY (2013) Recent advances in flexible sensors for wearable and implantable devices. J Appl Polym Sci 130(3):1429–1441. https://doi.org/10.1002/app.39461

Pudasaini PR, Sharma M, Ruiz-Zepeda F, Ayon AA (2014) Ultrathin, flexible, hybrid solar cells in sub-ten micrometers single crystal silicon membrane. In: 2014 IEEE 40th photovoltaic specialist conference (PVSC). IEEE, pp 0953–0955

Rao RA, Mathew L, Saha S, Smith S, Sarkar D, Garcia R, Stout R, Gurmu A, Onyegam E, Ahn D (2011) A novel low cost 25μm thin exfoliated monocrystalline si solar cell technology. In: 2011 37th IEEE photovoltaic specialists conference (PVSC). IEEE, pp 001504–001507

Shahrjerdi D, Bedell SW (2013) Extremely flexible nanoscale ultrathin body silicon integrated circuits on plastic. Nano Lett 13(1):315–320. https://doi.org/10.1021/nl304310x

Shahrjerdi D, Bedell SW, Khakifirooz A, Fogel K, Lauro P, Cheng K, Ott JA, Gaynes M, Sadana DK (2012) Advanced flexible CMOS integrated circuits on plastic enabled by controlled spalling technology. In: 2012 IEEE international electron devices meeting (IEDM). IEEE, pp 5–1

Suo Z, Hutchinson JW (1989) Steady-state cracking in brittle substrates beneath adherent films. Int J Solids Struct 25(11):1337–1353. https://doi.org/10.1016/0020-7683(89)90096-6

Takei K, Takahashi T, Ho JC, Ko H, Gillies AG, Leu PW, Fearing RS, Javey A (2010) Nanowire active-matrix circuitry for low-voltage macroscale artificial skin. Nat Mater 9:821–826. https://doi.org/10.1038/nmat2835

Tanielian M, Lajos RE, Blackstone S (1986) Method of making thin free standing single crystal films US patent US4582559A. https://patents.google.com/patent/US4582559A/en?oq=+4%2c582%2c559

Thouless MD, Evans AG, Ashby MF, Hutchinson JW (1987) The edge cracking and spalling of brittle plates. Acta Metall 35(6):1333–1341. https://doi.org/10.1016/0001-6160(87)90015-0

Weil R (1970) The origins of stress in electrodeposits. Part 1. Plating 57(12):1231–1237

Xu Y, Blume JA, Shih CF (1993) An interface crack between an orthotropic thin film and substrate. Int J Fract 63(4):369–381

Ying M, Bonifas AP, Lu N, Su Y, Li R, Cheng H, Ameen A, Huang Y, Rogers JA (2012) Silicon nanomembranes for fingertip electronics. Nanotechnology 23(34):344004. https://doi.org/10.1088/0957-4484/23/34/344004

Zhai Y, Mathew L, Rao R, Xu D, Banerjee SK (2012) High-performance flexible thin-film transistors exfoliated from bulk wafer. Nano Lett 12(11):5609–5615. https://doi.org/10.1021/nl302735f

Publisher's Note Springer Nature remains neutral with regard to jurisdictional claims in published maps and institutional affiliations.